Published online 1 December 2011 *Nucleic Acids Research, 2012, Vol. 40, No. 7* ***3117–3130***
doi:10.1093/nar/gkr1154

Multiple conformations of SAM-II riboswitch detected with SAXS and NMR spectroscopy

Bin Chen[1], Xiaobing Zuo[2], Yun-Xing Wang[2] and T. Kwaku Dayie[1,*]

[1]Department of Chemistry and Biochemistry, University of Maryland, College Park, MD 20742 and [2]Protein-Nucleic Acid Interaction Section, Structural Biophysics Laboratory, Center for Cancer Research, National Cancer Institute, National Institutes of Health, Frederick, MD 21702, USA

Received July 12, 2011; Revised November 9, 2011; Accepted November 10, 2011

ABSTRACT

Riboswitches are a newly discovered large family of structured functional RNA elements that specifically bind small molecule targets out of a myriad of cellular metabolites to modulate gene expression. Structural studies of ligand-bound riboswitches by X-ray crystallography and nuclear magnetic resonance (NMR) spectroscopy have provided insights into detailed RNA–ligand recognition and interactions. However, the structures of ligand-free riboswitches remain poorly characterized. In this study, we have used a variety of biochemical, biophysical and computational techniques including small-angle X-ray scattering and NMR spectroscopy to characterize the ligand-free and ligand-bound forms of SAM-II riboswitch. Our data demonstrate that the RNA adopts multiple conformations along its folding pathway and suggest that the RNA undergoes marked conformational changes upon Mg^{2+} compaction and *S*-adenosylmethionine (SAM) metabolite binding. Further studies indicated that Mg^{2+} ion is not essential for the ligand binding but can stabilize the complex by facilitating loop/stem interactions. In the presence of millimolar concentration of Mg^{2+} ion, the RNA samples a more compact conformation. This conformation is near to, but distinct from, the native fold and competent to bind the metabolite. We conclude that the formation of various secondary and tertiary structural elements, including a pseudoknot, occur to sequester the putative Shine–Dalgarno sequence of the RNA only after metabolite binding.

INTRODUCTION

S-Adenosylmethionine (SAM), as a major methyl donor, plays a central role in signal transduction and transcriptional regulation of many critical processes in sulfur metabolism of certain bacteria (1). While such regulatory mechanisms of feedback inhibition performed by proteins are sophisticated and have long been recognized (2,3), it is becoming increasingly clear that non-protein coding RNAs, such as riboswitches, also play an important role in the regulation of gene expression (4–8).

Riboswitches are structured functional RNA elements that are typically located at the 5′ non-coding regions of messenger RNAs (9) and comprise an aptamer domain and an expression platform domain. The aptamer domain functions as a sensor to recognize and specifically bind small molecule targets out of a myriad of intracellular metabolites, whereas the expression platform modulates gene expression in response to the binding events in the aptamer domain. It is thought that a change in conformation can lead to either inhibition of transcription elongation via formation of terminator structure or blockage of translation through sequestering of the ribosome binding site (4,10,11). This presumed regulatory strategy is likely achieved through the interplay of two mutually exclusive secondary structures of the expression platforms that lead to either expression or repression of the downstream genes encoding for the enzymes responsible for the transport or biosynthesis of the target metabolites (12,13).

Although significant progress has been made in understanding how riboswitches recognize their ligands (14–23), the nature of the unbound state is still not very well defined (24–28). Instead, several conflicting perspectives about the unbound state have arisen (27). First, both the apo and the bound states of a *Thermotoga maritima asd* lysine riboswitch have identical structures with the ligand binding pocket completely buried within the molecule, making it hard to rationalize how the ligand interacts with the riboswitch and enters into the binding pocket (22,29,30). In addition, nuclear magnetic resonance (NMR) spectroscopy and fluorescence studies of the *Bacillus subtilis queC* and *Fusobacterium nucleatum* preQ1 riboswitches have revealed that the receptors are unstructured in the absence of ligand binding and that addition of preQ1 induced secondary structural

*To whom correspondence should be addressed. Tel: +1 301 405 3165; Fax: 1 301 314 0386; Email: dayie@umd.edu

rearrangement and global changes in the architecture of the riboswitches to shut down gene transcription (21,31). Ligand-induced folding has been investigated thermodynamically and kinetically, but it is still unclear how the ligand can recognize such a disorganized binding pocket (31). Moreover, for translational acting riboswitches such as S_{MK} box (SAM-III), distinct mutually exclusive RNA conformations are differentially populated in the presence or absence of the metabolite. It remains unclear how the metabolite triggers a switch from a different structure to a complex and highly specific binding pocket (32–34).

To better understand the functional mechanism of a riboswitch and its folding pathway in the unliganded state, we analyzed a SAM-II riboswitch with a sequence located upstream of the *metX* gene (encoding homoserine acetyltransferase) from the Sargasso Sea metagenome (35). X-ray crystal structural analysis indicated that three helical elements, two loops and a classic H-type pseudoknot all come together to form an intricate tertiary structure with the SAM binding pocket located in the center of helix P2b (Figure 1) (23). Striking features of the SAM-bound RNA structure are that the helical segments stack upon each other to create an overall extended conformation and that the 3′-end corresponding to the Shine–Dalgarno (SD) sequence is stabilized by base-pairing and tertiary interactions with loop 1 (23). These, together with the RNAs binding selectivity and the fact that SAM-II is one of the only riboswitches containing the sequences of both the aptamer and the expression platform, make SAM-II an attractive system to investigate the dynamics and alternative conformational switching upon ion and SAM binding.

We hypothesized that the predicted ribosome binding site of the free form RNA is exposed and accessible to the ribosome for recognition and that the ligand-free SAM-II RNA adopts multiple conformations that are modulated by ions and ligands. In this study, we characterize the SAM-II riboswitch under different folding conditions using small-angle X-ray scattering (SAXS) combined with NMR spectroscopy. These data suggest that the RNA undergoes marked conformational changes upon Mg^{2+} compaction and SAM metabolite binding and that Mg^{2+} binding induces a state that is competent to bind metabolite. Only after metabolite binding does the formation of various secondary and tertiary structural elements including a pseudoknot occur to sequester the SD sequence of the RNA. In the course of this work, a similar study using fluorescence and NMR spectroscopy and single molecule fluorescence energy transfer (smFRET) imaging revealed a dynamic unliganded SAM-II riboswitch (36). Our work complements and extends this recent study in two important aspects: SAXS provides direct evidence for at least four conformational states of varying compactions; NMR analysis provides greater insights into the nature of the secondary and tertiary structural rearrangement of the RNA in the presence of Mg^{2+} ions and metabolite.

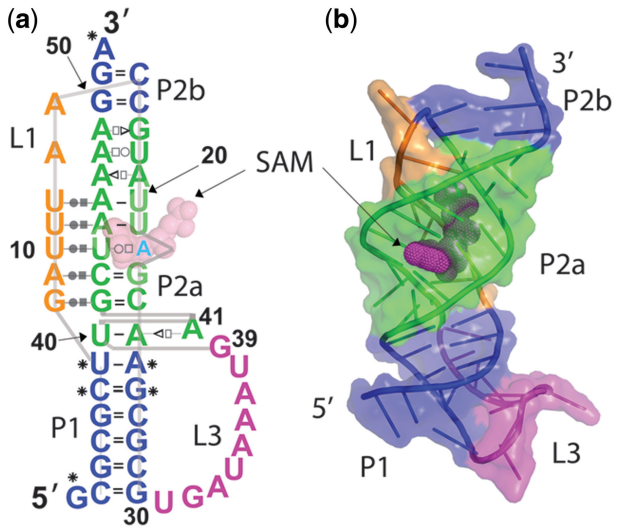

Figure 1. Secondary structure and X-ray crystal structure of SAM-II RNA (Protein Data Bank ID: 2qwy). (**a**) Metabolite-bound secondary structure of SAM-II riboswitch proposed from the X-ray crystal structure. The RNA used in this study has two single point mutations (U1G for improving transcription efficiency and G52A for enhancing 3′-end cleavage by the 3′ HδV ribozyme) compared with its wild-type. The X-ray structure contains two additional double point mutations (C6G U7C and A25G G26U) for adding a cesium/iridium ion binding site for phasing (23). These are indicated by asterisk. (**b**) X-ray crystal structure of SAM-II riboswitch with the same color coding as the secondary structure (Protein Data Bank ID: 2qwy) (23).

MATERIALS AND METHODS

Reagents and materials

Oligonucleotides for the polymerase chain reaction were purchased from Integrated DNA Technologies, Inc. The SAM was obtained from Sigma and *Taq* DNA polymerase from New England Biolabs, Inc. A plasmid containing the SAM-II RNA sequence along with a self-cleaving transacting HδV ribozyme at the 3′-end was a gift from Dr Robert T. Batey of the University of Colorado at Boulder.

RNA preparation

The RNA used in this study is a variation of the wild type RNA described by Gilbert *et al.* (23), in which two single point mutations were introduced to change uracil 1 to guanine for improving transcription efficiency and guanine 52 to adenine for enhancing 3′-end cleavage by the 3′ HδV ribozyme. The RNA was transcribed as described.

Size-exclusion chromatography

Chromatographic separation was performed with the ÄKTA™ Design system with a detector at a wavelength of 254 nm. The conformational homogeneity of the RNA sample was checked using size exclusion chromatography (SEC) with a Superdex 200 HR 10/30 column (GE Healthcare; column height: 30 cm, column diameter: 1.0 cm, column volume: 23.562 ml). Samples of SAM-II riboswitch in 50 mM sodium−2-(*N*-morpholino)ethanesulfonic acid (Na-MES), pH 6.2, 50 mM NaCl were

denatured at 90°C for 3 min, snap cooled and incubated on ice for 10 min, then Mg^{2+} and/or the metabolite of varying concentrations were added, and the mixtures were incubated on ice for 30 min before loading onto the column. A flow rate of 0.5 ml/min was used in all the chromatographic steps performed at 4°C.

Electrophoretic mobility shift assay

Samples of SAM-II riboswitch used in electrophoretic mobility shift assay were prepared as described above. Electrophoresis was performed using 12% native polyacrylamide gel electrophoresis (PAGE) in 90 mM Tris, 90 mM MES, pH 8.0, in the absence or presence of 50 mM NaCl and varying concentrations of $MgCl_2$ or the metabolite at 4°C at 300 V. The RNA samples and gel matrix contained identical concentrations of $MgCl_2$ and the metabolite, and running buffer was kept recirculating every 1 h. The gels were stained with ethidium bromide and images were scanned on a STORM phosphoImager (GE Healthcare).

Small angle X-ray scattering experiments and data analysis

Both SAXS and wide angle X-ray scattering (WAXS) data were collected at beam line 12-ID of the Advanced Photon Source at the Argonne National Laboratory. The wavelength, λ, of the X-ray radiation was set to 1.033 Å. Detailed protocols of SAXS measurement have been described elsewhere (37). In brief, the SAM-II riboswitch RNA was dissolved in buffer A (50 mM Na-MES at pH 6.2). Samples were heated at 90°C for 3 min followed by cooling on ice for 10 min. $MgCl_2$ and/or SAM ligand were added to prepare four RNA sample buffer conditions: A1 (buffer A without $MgCl_2$ or ligand), A2 (buffer A with 10 mM $MgCl_2$), A3 (buffer A with 0.5 mM ligand) and A4 (buffer A with 10 mM $MgCl_2$ and 0.5 mM ligand). To ensure identical buffer conditions, each sample was then exchanged with the appropriate buffers (A1–A4) six times using an Amicon microconcentrator filter (Millipore). RNA samples were prepared in three concentrations (0.8, 1.8 and 3.6 mg/ml) for each of the four buffer conditions before shipping on dry ice, therefore, making a total of 12 samples.

The q-range used for data analysis was between 0.006 and 0.300 $Å^{-1}$. The linearity of the Guinier plot was used to evaluate the quality of the SAXS data. WAXS data were used to guide accurate background subtraction for the corresponding SAXS data (38). A total of 20 images were taken for each sample condition to get good statistics and converted to 1D scattering profiles. The resulting scattering data sets were averaged before buffer background subtraction using IGOR PRO (WaveMetrics) software. The reported radius of gyration (R_g) values were derived from a Guinier approximation in the q-range such that $q_{max} \times R_g < 1.3$. The GNOM software (39) was used to determine R_g values, which were in good agreement with those obtained from Guinier analyses. This software was also used to perform pair distance distribution function (PDDF) plots.

Low resolution *ab initio* model reconstructions of SAM-II riboswitch

GNOM (39), DAMMIN (40) and DAMAVER (41) from the ATSAS 2.4 suite of programs were used to perform *ab initio* model reconstructions of the RNA under the four solution conditions described above. To avoid underestimation of the molecular dimension, we chose the parameter R_{max}, the upper end of distance r, such that the resulting PDDF has a short, near-zero-value tail at large r. The maximum distances (D_{max}) were estimated to be 112, 72, 70 and 68 Å from the PDDF for the SAM-II RNA under the four experimental conditions (see 'Results' section). We used the program DAMMIN to obtain an approximate molecular envelope. To avoid distortion caused by possible underestimation of D_{max}, we usually set the R_{max} to be about 10 Å greater than D_{max}. All reconstructions for SAM-II under the four conditions were performed in the 'slow' mode. The resulting structural models were averaged using the program package DAMAVER (41), which generates an average and filtered dummy atom model. In this program, the normalized spatial discrepancy (NSD) values between each pair of models were computed. The model with the lowest average NSD with respect to the rest of the models was chosen as the reference model. The remaining models were superimposed onto the reference model using SUPCOMB. Possible outliers identified by NSD criteria were discarded. A total of 20 independent DAMMIN runs were performed, and the resulting bead models were averaged using DAMAVER. CRYSOL (42) was used to calculate the R_g value and the SAXS profile for the SAM-II crystal structure.

NMR sample preparation and NMR experiments of SAM-II RNA

The purified RNA was lyophilized and dissolved in water, and the corresponding amount of buffer stock solutions was added. The RNA sample solutions were refolded using identical conditions as described above. Then 8–10% D_2O and various concentrations of SAM ligand and Mg^{2+} were added and the sample volume was adjusted to 260 µl with ddH_2O in Shigemi NMR tubes. The final NMR buffer contains 10 mM sodium phosphate, pH 6.2 and 100 mM NaCl. The sample concentration was ~0.5−1 mM for NMR experiments as judged by the magnitude of UV absorbance at 260 nm and the calculated extinction coefficient (668 300 $M^{-1}cm^{-1}$) of the individual RNAs base composition.

NMR experiments were performed on a Bruker Avance 600 MHz spectrometer equipped with actively shielded z-axis gradient triple resonance probe. NMR spectra were recorded at a temperature of 298 K using the WATERGATE water suppression pulses (43). $^{1}H-^{15}N$ HSQC, $^{1}H-^{13}C$ HSQC, $^{2}J_{HN}-^{1}H-^{15}N$ HSQC (44) and 2D NOESY experiments were carried out using standard pulse sequences (45). The $^{2}J_{NN}-HNN-COSY$ experiments were performed as described (46). Homonuclear NOESY spectra used to determine imino proton connectivities were recorded with a mixing time of 300 ms, with 256 complex points in the indirect dimension.

$^{1}H-^{15}N$ HSQC spectra were recorded with 256 complex points in the indirect dimension. All spectra were processed and analyzed using Bruker's TOPSPIN 2.1, NMRPipe/NMRDraw (47) and NMRView (48).

RESULTS

We first performed conformational heterogeneity analysis of the SAM-II RNA sample under different solution conditions using analytical SEC and electrophoretic mobility shift assay in the absence or presence of Mg^{2+} and/or SAM metabolite. SAXS data were then collected on SAM-II riboswitch in the absence or presence of Mg^{2+} and/or SAM metabolite. Based on the SAXS data, we reconstructed four *ab initio* low-resolution electron density models corresponding to four different folding states of the RNA. Finally, we characterized the free and native states of the RNA using NMR spectroscopy to complement the SAXS data. Models for the RNAs folding and regulatory mechanism were proposed based on our data.

Conformational heterogeneity analysis of the RNA sample

Preparation of homogenous macromolecule samples is critical for biochemical and biophysical studies. Generally, RNA synthesis involves several steps including an *in vitro* transcription with T7 RNA polymerase, purification by a denaturing PAGE, dialysis and buffer exchange and storage at −20°C, denaturation and renaturation before biochemical and biophysical studies. This production protocol, although robust and well-established, suffers from several disadvantages in addition to probable aggregation of RNA samples (49). First, RNA molecules derived from denaturing PAGE purification contain acrylamide oligomer contaminations that will interfere with the SAXS scattering analysis and compromise interpretation of NMR data (50,51). Second, RNA molecules, as a result of the renaturation process, may misfold into kinetically trapped species that can result in conformational heterogeneities (51–53). However, accurate SAXS data interpretation and model reconstruction require homogenous samples with defined conformers in solution because the intensity of the scattering data results from population weighted averages of parameters from individual components (54). As a result, conformational heterogeneity of the RNA increases the possibility of misinterpretation of SAXS data, leading to reconstruction of artifactual bead models.

To avoid this problem, we examined the conformational homogeneity of the SAM-II RNA before SAXS analyses using SEC on fast performance liquid chromatography (FPLC). The RNA was first synthesized by *in vitro* transcription with T7 RNA polymerase and purified by denaturing PAGE to homogeneity. A folding protocol of snap-cooling on ice after denaturing at 90°C for 3 min was used to test its effect on the RNA folding in the absence or presence of Mg^{2+} ion and/or SAM metabolite. The elution profile of the SEC run shows a single peak of the SAM-II RNA in the absence of Mg^{2+} and metabolite, indicating that no minor conformer exists or were too insignificant to be detected under our experimental conditions (Figure 2a).

More analytical SEC analyses were conducted for the RNA in the presence of different concentrations of Mg^{2+} ion and/or saturating amounts of metabolite to examine the conformational homogeneity of the RNA under these solution conditions. An overlay of SEC chromatograms of the RNA in the presence of different Mg^{2+} ion concentrations as a function of retention time reveals that no shoulder peak is present, an indication that the RNA is a monomer and homogenous under all of the solution conditions (Figure 2b). In the absence of Mg^{2+}, the SAM-II riboswitch elutes from the column at ~14.5 ml. Addition of 1 mM Mg^{2+} ion to the mobile phase resulted in a slight delay in the retention time, suggesting a decrease of particle hydrodynamic radius. As the Mg^{2+} concentration increases, the RNA elutes with longer retention time from the column. Compaction of SAM-II riboswitch as a function of Mg^{2+} concentration reveals a folding transition with $Mg_{1/2} \approx 6$ mM (Figure 2c). Similar compaction was also observed for the RNA in the presence of saturating amount of the metabolite (Figure 2d), monovalent ion or other divalent ion such as Ca^{2+} (Supplementary Figure S1). This is most likely because the Mg^{2+} or metabolite induced compaction of the RNA caused a decrease in particle size, making the RNA travel a more circuitous path through the SEC stationary phase, and as a result exhibited a delay in retention time. Given the different behaviors of RNA and protein on SEC, this delay suggested remarkable changes of the particle size or hydrodynamic radii, although there is no standard curve for single-stranded RNA on a Superdex 200 (10/30) column to quantitatively monitor the change of the hydrodynamic radius (55). As a second method, the RNA was analyzed on native PAGE under a series of Mg^{2+} ion and/or the metabolite concentrations to examine their effects on the folding and conformational change of the RNA.

Native gel mobility shift assay

Native PAGE is a simple but useful technique to test RNA folding and conformational changes at a gross level, and therefore applicable to riboswitches that change conformation upon binding metal ions or specific metabolites. If an alternative state of the RNA is present after refolding and the exchange between the two states is slow relative to the migration rate of the RNA through the gel, then bands with different migration rates will be observed, corresponding to different conformational states; otherwise, a single band of average mobility will be observed (56). As reported by Batey's group, the binding affinity between the SAM-II riboswitch and the metabolite is high (in the low micromolar range) in the presence of magnesium ions, indicating that once bound to the metabolite, the RNA likely adopts a compact conformation that should migrate more rapidly through the gel than the unbound RNA (57).

An estimate of the relative migration rate of the SAM-II RNA was obtained by comparing the native gel electrophoretic mobilities in the absence or presence of Mg^{2+} or

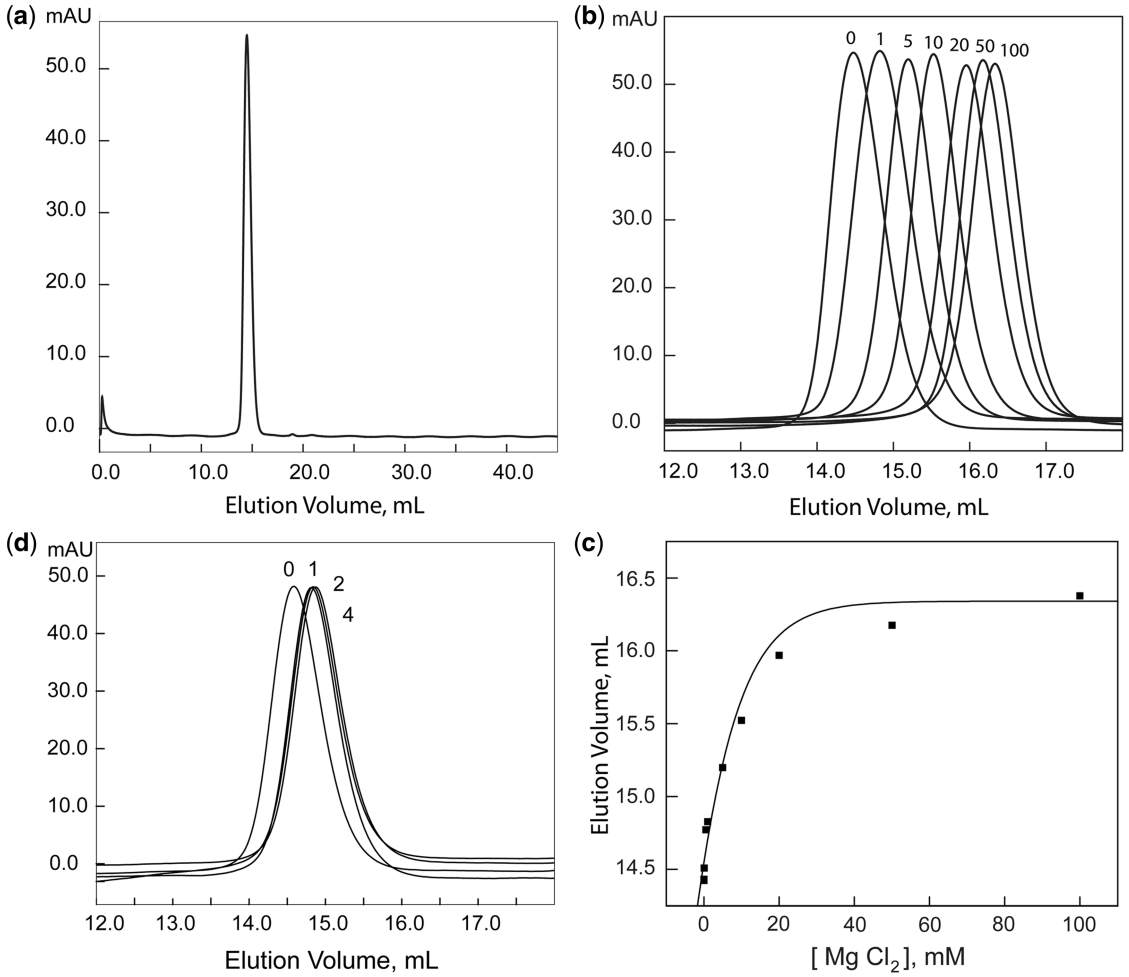

Figure 2. Analysis of the homogeneity and conformation of the SAM-II RNA. (**a**) SEC elution profile for SAM-II riboswitch in the absence of Mg^{2+} ion and the metabolite. (**b**) SEC elution profiles for SAM-II riboswitch in the presence of different concentrations of Mg^{2+} ion (mM) in the mobile phase. Increasing $MgCl_2$ concentration resulted in preferential retention of the SAM-II riboswitch on the column, presumably because of decreasing hydrodynamic radius. (**c**) Compaction of SAM-II riboswitch as a function of $MgCl_2$ concentration reveals a folding transition with $Mg_{1/2} = 6$ mM. (**d**) SEC elution profiles for SAM-II riboswitch in the presence of different molar ratios of the metabolite to SAM-II riboswitch. Addition of the metabolite caused a delay in the retention time of the RNA, consistent with a decrease in hydrodynamic radius of the RNA. Vertical axes for (a), (b) and (d) are in mAU at 254 nm.

different stoichiometric amounts of the SAM metabolite (Figure 3). In the absence of Mg^{2+} ion and metabolite, the RNA exhibits a homogenous single band. Addition of different stoichiometric amounts of the metabolite, in the absence of Mg^{2+} ion, did not change the electrophoretic mobility of the RNA (Figure 3a). In the presence of 0.2 mM Mg^{2+} without the metabolite, the RNA migrates as a homogenous band again. However, in the presence of unsaturating metabolite, the RNA adopts two conformations: an unbound form and a compact conformation. Upon adding saturating amount of the metabolite, the RNA switches completely to the compact conformation and the relative electrophoretic mobility of the compact complex is substantially accelerated. Consequently, it migrates more rapidly compared with the unbound RNA molecules. In the presence of 1 mM Mg^{2+} and different stoichiometric amounts of the metabolite, the RNA exhibits similar migration patterns to that observed in the presence of 0.2 mM Mg^{2+} (Figure 3a), suggesting that the metabolite plays a critical role in RNA conformational change in the presence of low Mg^{2+} ion concentration. Using bromophenol blue as a standard, we compared electrophoretic mobilities of different bands to that of the dye to obtain relative mobility (R_f) values. Notably, the R_f values of the RNA are different in the absence or presence of different Mg^{2+} ion concentrations, indicating that Mg^{2+} ion indeed plays a key role in promoting compaction of the RNA molecule. Surprisingly, in the presence of 10 mM Mg^{2+}, the relative electrophoretic mobilities of the RNA bound to different stoichiometric amounts of metabolite are nearly identical (Figure 3a). These observations suggest that at high Mg^{2+} concentrations, the RNA molecule is already compacted to such an extent that addition of the metabolite has only an incremental effect on further folding the RNA, consistent with the results from SEC analyses.

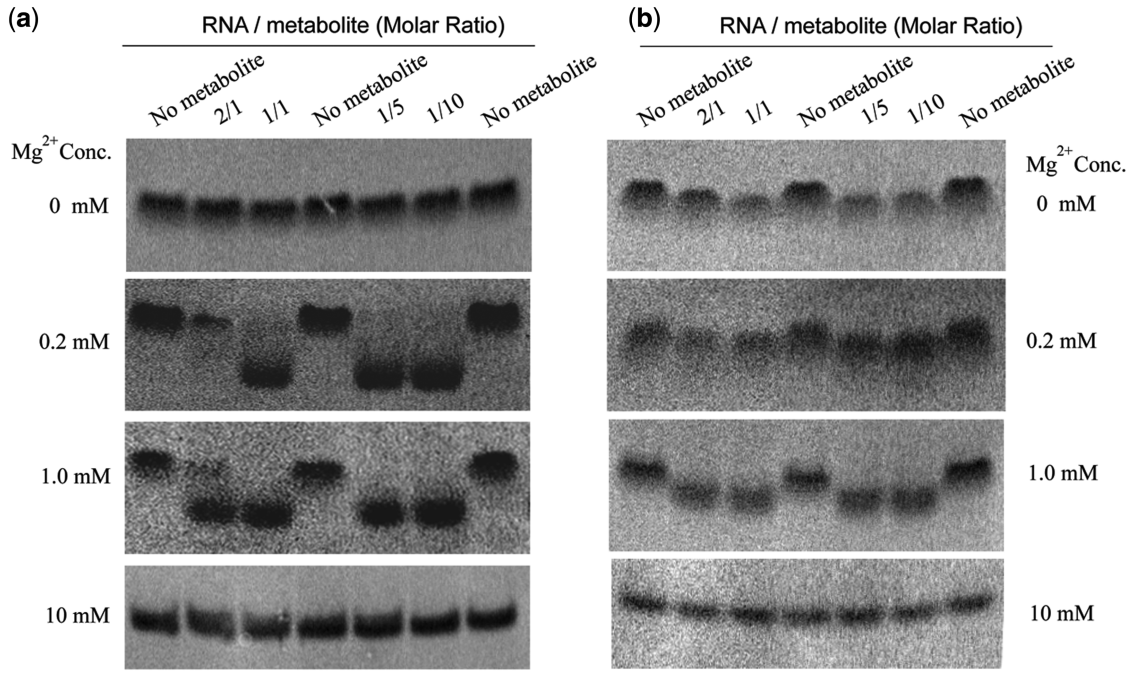

Figure 3. Native PAGE of SAM-II riboswitch in 90 mM Tris•MES, pH 8.0 in the absence (**a**) and presence (**b**) of 50 mM NaCl. 2/1, 1/1, 1/5 and 1/10 indicates the molar ratios between the RNA and the SAM metabolite.

The mobility shift pattern is slightly different in the presence of 50 mM Na^+ ion. The RNA shifts negligibly upon addition of the metabolite in the absence of Mg^{2+} ion. In the presence of 1 mM Mg^{2+} ion, the metabolite-induced migration shift is not as dramatic as that observed in the absence of 50 mM monovalent (Figure 3b). Taken together, these data suggest that substantial rearrangement of the RNA occurs upon binding saturating amount of the metabolite or high concentration Mg^{2+} ion and reveal that the RNA adopts different conformations in the absence or presence of Mg^{2+} and saturating amount of metabolite. The native gel shift assay provides a hint about big conformational changes. Further studies to address and provide models of the riboswitch folding as a function of Mg^{2+} and the metabolite by using SAXS and NMR analysis, however, indicate that there are still some conformational differences of the RNA under the conditions.

Following the conformational changes of the SAM-II riboswitch induced by the metabolite and Mg^{2+} ion with SAXS

Solution scattering profiles were collected on SAM-II riboswitch in the absence or presence of 10 mM Mg^{2+} and 0.5 mM SAM metabolite after passing the samples through a gel filtration column to ensure that the RNAs were monomeric and conformationally homogeneous. Four scattering curves representing the four buffer conditions described earlier (A1–A4) that were overlaid exhibited significant differences, indicating the existence of four possible conformational states along the RNA-folding pathway (Figure 4a). The SAXS data were analyzed using the linearity of the Guinier plot (a plot of natural log intensity [log I(q)] versus q^2, where q is the momentum transfer). From the scattering data, the R_g was calculated at low q values in the range of $qR_g < 1.3$, using the Guinier approximation: $\ln[I(q)] \cong \ln[I(0)] - R_g^2 q^2/3$. The data reveals that the R_g of the SAM-II riboswitch changes dramatically with the four sample conditions. In the absence of Mg^{2+} and the metabolite (condition A1), the RNA adopts an extended conformation, which we call the unfolded state (U) under low-salt condition (50 mM Na^+) with an R_g of 31.7 Å. In the presence of 10 mM Mg^{2+} (condition A2), R_g decreases to 21.5 Å which we designate as a compact intermediate state (M). Further compaction of R_g to 20.7 Å occurs in the presence of 0.5 mM metabolite without Mg^{2+} (condition A3) to give a conformation referred to as the bound state (B). Finally, in the presence of both Mg^{2+} and the metabolite (condition A4), R_g compacts even further to 19.5 Å which we denote as the native folded state (N) (Table 1). Compared with the R_g value of ~19 Å calculated from a 2.8-Å-resolution X-ray crystal structure in metabolite-bound form of SAM-II RNA (23), the R_g of 31.7 Å of the RNA in the absence of Mg^{2+} and the metabolite is considerably larger, suggesting that the RNA under this solution condition is extended. To further derive the degree of RNA compaction and highlight RNAs with large unfolded regions, the SAXS data were transformed into Kratky representations (Figure 4b), where the scattering intensity is weighted by the square of the momentum transfer (q) ($I \times q^2$ versus q). According to Porod's law, the scattering profiles from folded proteins or nucleic acids with a well-defined surface fall approximately as q^{-4} at large q and the profiles therefore tend to have a pronounced peak in the Kratky representation. In contrast, completely unfolded

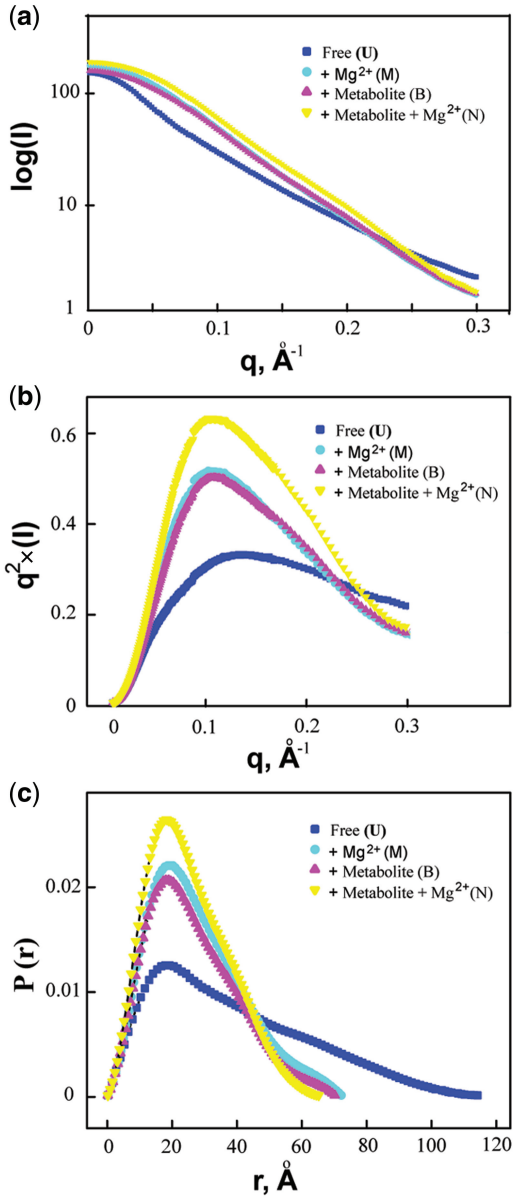

Figure 4. SAXS analysis of SAM-II RNA under four different states. (**a**) Comparison of experimental scattering profiles of SAM-II. The experimental curves were placed on a relative scale in origin. (**b**) Comparison of the SAXS data in Kratky representation for SAM-II under the four states. (**c**) Comparison of $P(r)$ determined from experiments using GNOM for the four different states.

polymers show a linearly rising scattering curve (58). The scattering curve of SAM-II RNA under the condition of 50 mM Na-MES buffer without added Mg^{2+} or metabolite exhibits a flattened plateau with scattering intensity falling slightly at large angles. Although it is different from an upward rising scattering intensity representative of a completely denatured conformation, it is consistent with a partially 'unfolded state' with an extended conformation. This extended conformation is better visualized by comparing the distance distribution PDDF $P(r)$, which provides information on the shape and maximum intramolecular distance of the particles (58,59). The RNA in U state has a remarkably larger maximum intramolecular distance D_{max} of 112 Å than other states as presented in Table 1 and Figure 4c. This D_{max} value, compared with the size and the length expected from the SAM-II RNA crystal structure further confirms that the RNA conformation in the U state is not a completely denatured random coil, attributed to its partially formed secondary structure.

Upon addition of 10 mM Mg^{2+} to the U state, the RNA undergoes significant compaction with a decreased R_g from 31.7 to 21.5 Å and a decreased maximum intramolecular distance D_{max} from 112 to 72 Å, indicating the population of a more compact 'intermediate state' (M state) that is near folded as confirmed by the appearance of a concave peak in the Kratky plot. This compact M state was also observed in the scattering profile of the RNA in the presence of 2 mM Mg^{2+} without metabolite (Supplementary Figures S2 and S3), suggesting that the M state is likely fully populated under these solution conditions and that high stabilizing Mg^{2+} ion concentrations induce global collapse and structural rearrangement of the RNA in the absence of the metabolite. The monovalent and divalent ions effectively screen the negatively charged backbone of the RNA, facilitating and stabilizing as yet unidentified long-range or tertiary contacts within an electrostatically relaxed conformation (60–63).

Remarkably, in the presence of low concentration of monovalent ions (50 mM Na^{+}) and 0.5 mM SAM metabolite but in the absence of Mg^{2+} ions (B state), the scattering pattern is similar to that of the M state, with an R_g value of 20.7 Å and a maximum intramolecular distance D_{max} of 70 Å. However, this B state is distinguishable from those in U and N states, from NMR analysis (see below). As indicated earlier, addition of both 0.5 mM metabolite and 10 mM Mg^{2+} resulted in further compaction

Table 1. Overall parameters and quality indicators derived from the scattering data for the SAM-II riboswitch under different conditions

Structural properties of the RNA under different thermodynamic states				
States	Solution conditions	R_g (Å)	D_{max} (Å)	NSD
Unfolded (U)	Buffer	31.7 ± 0.5	112	0.68 ± 0.01
Intermediate (M)	Buffer + 10 mM Mg^{2+}	21.5 ± 0.2	72	0.62 ± 0.03
Bound (B)	Buffer + 0.5 mM SAM	20.7 ± 0.2	70	0.65 ± 0.02
Native (N)	Buffer + 10 mM Mg^{2+} + 0.5 mM SAM	19.5 ± 0.2	68	0.62 ± 0.04

The R_g calculated from the crystal structure (Protein Data Bank ID: 2qwy) is ~ 19 Å and the maximum intramolecular distance of the crystal structure is 67 Å. The R_g were fit by Guinier analysis of the low angle scattering data, and the maximum intramolecular distances (D_{max}) were obtained using the program GNOM. The NSD values of the four low resolution reconstruction models were generated from the program DAMAVER. The buffer is 50 mM Na-MES (pH 6.20).

of R_g to 19.5 Å with the smallest D_{max} of 68 Å. This value of R_g is in good agreement with the R_g (~19 Å) calculated from the crystal structure (Table 1) (23). Comparison of the scattering profiles for the B, M and N states indicates that the reduction of R_g is accompanied by a small conformational change of the RNA. A sharp peak in the Kratky representation of the scattering curve in the N state demonstrates that the RNA under this solution condition is in its native tertiary conformation with a well-defined molecular surface (58).

Low resolution *ab initio* modeling

To better visualize the conformational changes, we constructed *ab initio* models of the SAM-II RNA in the four states by using a low resolution structure reconstruction method based on the SAXS data using the program DAMMIN (see 'Materials and Methods' section) (40). A total of 20 independent DAMMIN runs were performed for each of the four models corresponding to the four states. The resulting 20 models were averaged using the program package DAMAVER (41). In this program, the NSD between each pair of models was computed. NSD provides a quantitative estimate of similarity between models: identical models give an NSD of zero, similar models give NSD values ≈ 1, while models with different shapes give NSD values greater than one (64). The final low-resolution reconstruction obtained represents the average molecular envelope of the ensemble.

The average NSDs for the four reconstructions are 0.68, 0.62, 0.65 and 0.62, indicating excellent convergences in both individual DAMMIN fits and overall bead model ensembles for the RNA under these four different states. The low-resolution models corresponding to the four states are presented in Figure 5a, which shows different views of the final surface of the *ab initio* models (molecular envelope) as mesh representations with 'filtered' models rendered as beads and aligned inside the molecular envelopes.

The U state reconstruction reveals an elongated conformation with a D_{max} of 112 Å. Based on the secondary structure derived from the X-ray crystal structure, we assume that the P1 stem is robustly formed in the U state RNA, as it is the most established secondary structure involving six successive base pairs, and the 3′ tail of the RNA starting from U31 adopts an open, elongated conformation without any secondary or tertiary contacts with other parts of the RNA. The P1 stem is located near the middle section of the reconstruction with a big loop from G8 to A24 at one end and the 3′ tail at the other. The width of the middle section of the elongated reconstruction is ~20 Å, consistent with that of a standard double stranded helix from an A form RNA, confirming the assumption of the existence of a helical stem along the RNA molecule. Although it is hard to calculate accurately the length of the extended structure, the D_{max} of 112 Å generated from the scattering data is in the right range of molecular length. The pairwise NSD values of 0.66–0.72 of the U state reconstructions indicate that the 20 models generated from the scattering profile exhibit quite similar elongated shape, rather than adopting various conformations such as bending or twisting, most likely due to electrostatic repulsion under the low salt condition used here (65).

The models for the other states exhibit more compact conformations with significantly reduced D_{max} values (72, 70 and 68 Å for M, B and N states, respectively), and their molecular shapes suggest that Mg^{2+} and/or the metabolite induced molecular compaction may bring about some tertiary interactions or possibly an increased extent of secondary structure, as shown by NMR below. The N state models show the lowest average NSD value, consistent with what we expected to be the most rigid and folded surface. Interestingly, the reconstructions from M state also show the same lowest average NSD, an indication that in the presence of 10 mM Mg^{2+} the loop region and the 3′ terminal is highly restrained. The B state reconstructions give average NSD value of 0.65, suggestive of a larger conformational variation in the absence of Mg^{2+} than that of M and N states (Figure 5a).

Comparison between the N state low resolution *ab initio* model and X-ray crystal structure

To ascertain whether SAXS can provide some tertiary structural information, we analyzed the scattering profiles from the solution N state and from X-ray structure (23). We calculated the scattering data from the SAM-II structure determined by X-ray crystallography using the program Crysol V. 2.6 and fitted it to the N state experimental SAXS curve (Figure 5b) (42). In addition, we superimposed the X-ray crystal structure (blue ribbon) with the N state *ab initio* model in surface (Figure 5c) representation (the 'filtered' model are rendered as beads aligned inside the envelope) using SUPCOMB20 (64). The excellent match between the curves and structural alignment between the X-ray structure and the 'filtered' model indicated that SAXS not only provided shape information but also identified the known structure in solution.

We observed a small discrepancy between the model and the X-ray structure (Figure 5c). The metabolite bound RNA in the crystal structure adopts an even more compact conformation than the N state RNA, as evidenced by a smaller R_g value and a smaller maximum intramolecular distance from the X-ray structure (Table 1). The tiny divergence might possibly result from different experimental conditions. Nonetheless, the RNA in solution N state adopts a compact conformation nearly identical to that of the X-ray crystal structure.

Role of Mg^{2+} ion in secondary and tertiary structural stabilization is pivotal for the RNA to adopt well-organized tertiary structure

Compared with the SAXS data from B state, the slight increase of R_g and D_{max}, but otherwise similar scattering curve in Kratky plot presented in Figure 4b and global shapes shown in Figure 5a, reveals that the conformation of the fully populated intermediate M state is nearly identical to the bound form, suggesting that either Mg^{2+} or the metabolite can cause compaction of the overall global shape and size of the RNA particle. However, SAXS

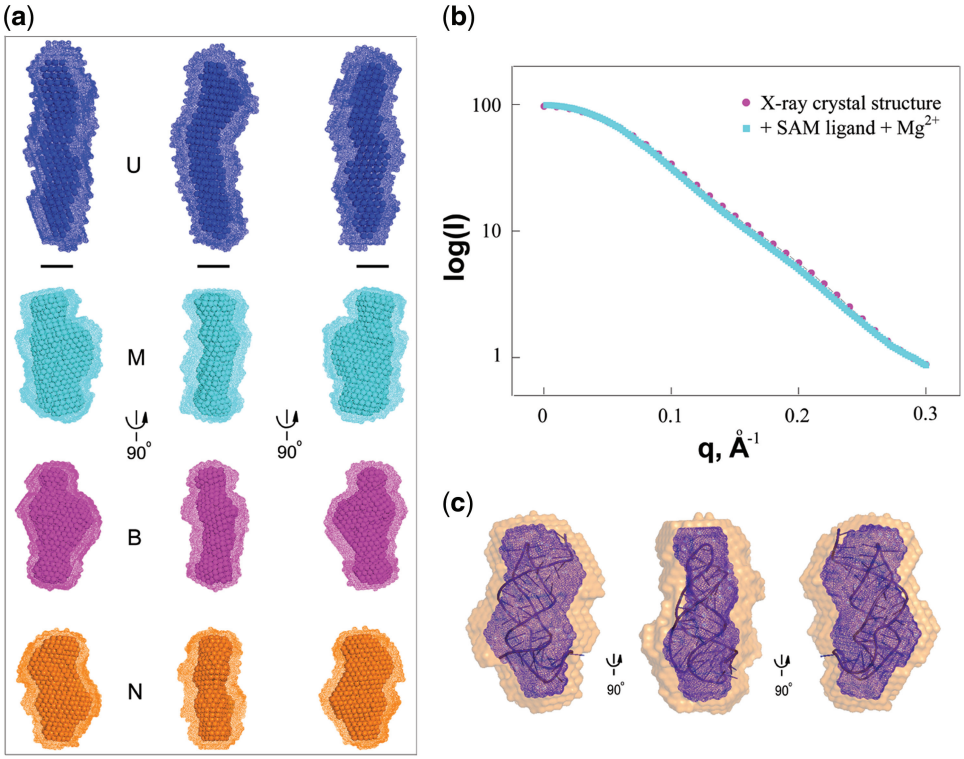

Figure 5. Low-resolution *ab initio* models of the SAM-II aptamer domain. (**a**) Average low-resolution *ab initio* models of the RNA under four different folding states: unfolded conformation (first row, blue, U state), conformation in the presence of 10 mM Mg^{2+} (second row, cyan, M state) and in the presence of 0.5 mM SAM metabolite (third row, magenta, B state) and low-resolution reconstruction in the presence of both 10 mM Mg^{2+} and 0.5 mM SAM metabolite (fourth row, brown, N state). Three different views are shown for the final consensus models (molecular envelope) as mesh representations with 'filtered' models rendered as beads aligned inside the molecular envelopes. The black scale bars represent 20 Å, the diameter of an A-form RNA helix, suggestive of the presence of such helices even in U state. (**b**) Experimental SAXS profile of SAM-II RNA in the presence of the metabolite and 10 mM Mg^{2+} (cyan) overlaid with the theoretical scattering profile (magenta) calculated from the X-ray crystal structure (Protein Data Bank ID: 2QWY). The experimental profile was placed on a relative scale in origin, and the theoretical profile was manually adjusted to illustrate the agreement with the experimental profile. (**c**) X-ray crystal structure (blue ribbon) superimposed with the *ab initio* model in the N state calculated from the experimental SAXS data as surface representation with 'filtered' models rendered as beads aligned inside the molecular envelopes. The alignments were performed with SUPCOMB20.

does not give any detailed indication of the changes in secondary or tertiary structure. Therefore, NMR titration experiments were performed to determine whether the Mg^{2+} and/or the metabolite induced structural rearrangements resulted in any changes of secondary structural elements. NMR chemical shift perturbation experiments are widely used to map and define binding sites in biomolecular complexes, especially in the case of RNA for measuring characteristic imino proton and monitoring the formation and breakage of Waston–Crick base pairs to define conformational change upon interacting with metabolites or metal ions (66). 1D NMR spectra of the titration of the riboswitch with Mg^{2+} ion in the absence of metabolite reveals that no major changes to the dispersion pattern of the imino protons (no chemical shift perturbation to the existing imino peaks and no strong new signals) occur, except of the appearance of one broadened but detectable imino signal, even upon addition of 8 mM Mg^{2+}, indicating that this compaction process does not involve any strong base pairing interactions, but results from Mg^{2+} mediated electrostatic interactions or unidentified tertiary interactions (Figure 6a). Although the Mg^{2+} collapsed state has an overall structure similar to those of bound form (B state) and native form (N state), it is a non-native conformation.

With titration of the RNA with different stoichiometric amounts of the metabolite in the presence of Mg^{2+}, however, a number of new imino protons peaks characteristic of canonical or non-canonical Watson–Crick base paring appear between 12 and 14.5 ppm, and many proton signals resonate around 9 ppm, even upon addition of 0.5 mM unsaturating amount of metabolite, demonstrating that the metabolite-induced compaction in the presence of Mg^{2+} indeed involves the formation of new base pairing interactions that increases the extent of helix packing and that are absent in the M state structure (Figure 6b).

We also carried out NMR titration experiments of the RNA with the metabolite in the absence of Mg^{2+}, and the results again demonstrated that this compaction process induced by the metabolite alone is associated with changes in base pairing with regards to the appearance of new imino signals. Further titration of the RNA with Mg^{2+} ion in the presence of the metabolite was performed.

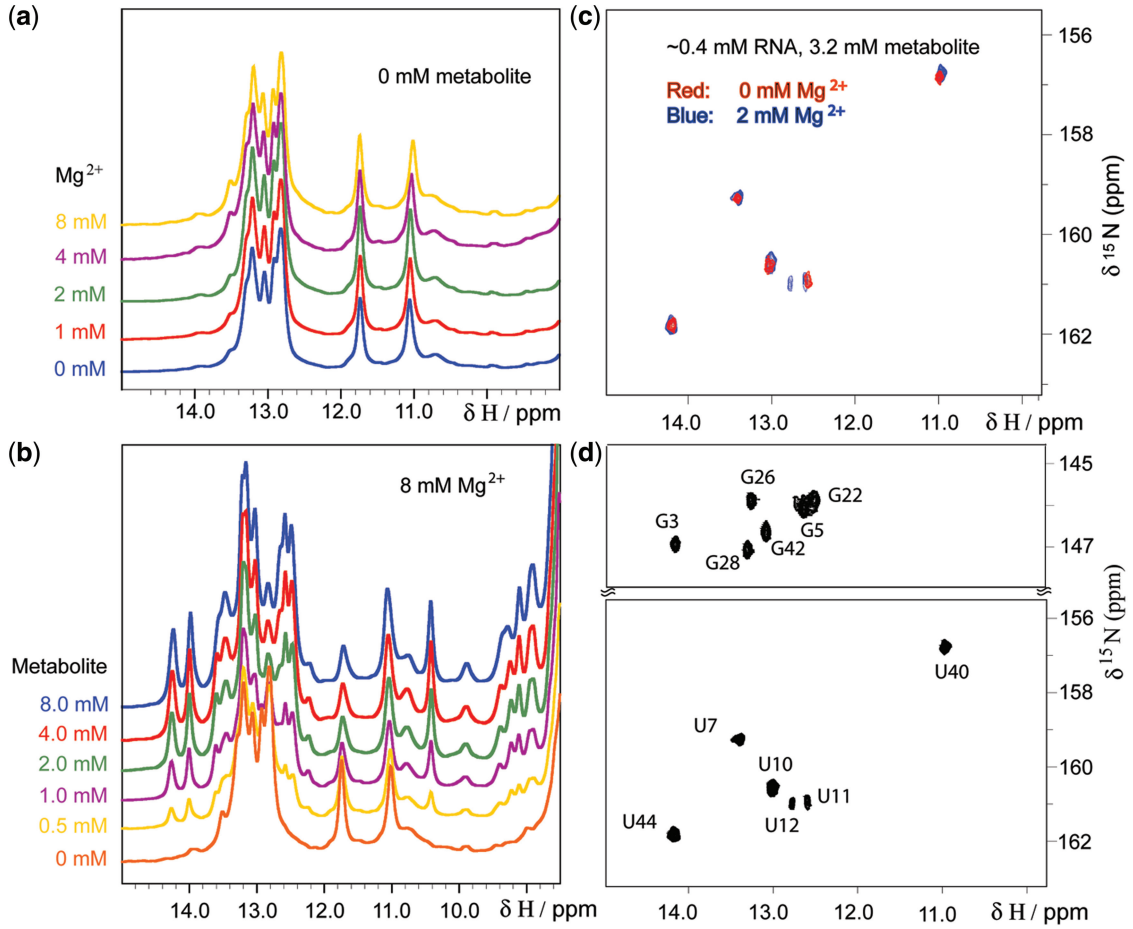

Figure 6. NMR spectra of SAM-II at 25°C reveal that both Mg^{2+} and the metabolite are required to drive folding of the RNA to the native state. (**a**) The imino region of 1D ^{1}H spectra of metabolite-free RNA with different concentrations of Mg^{2+} ion. (**b**) The imino region of 1D ^{1}H spectra of SAM-II riboswithc in the presence of 8 mM Mg^{2+} with different concentrations of the metabolite. (**c**) Imino region of the overlaid 2D $^{1}H-^{15}N$ HSQC spectra of $^{13}C,^{15}N$-uridine-labeled SAM-II riboswitch recorded at 0 or 2 mM Mg^{2+} concentrations conditions in the presence of 3.2 mM SAM ligand. (**d**) 2D imino $^{1}H-^{15}N$ HSQC spectrum of $^{13}C,^{15}N$-fully-labeled SAM-II riboswitch in the presence of 3.2 mM SAM ligand and 2 mM Mg^{2+} ion.

Figure 6c depicts an overlay of two imino $^{1}H-^{15}N$ HSQC spectra of $^{13}C/^{15}N$-A, U-labeled SAM-II RNA recorded at different concentration of Mg^{2+} ion. In the absence of both Mg^{2+} and metabolite, only 1 weak uridine imino crosspeak at ~13.4 ppm is present (Supplementary Figure S4). This is the only uridine present in helical stem P1. Note also that all the G–C base pairs in helix P1 are already formed in the absence of both Mg^{2+} ions and metabolite. In the absence of Mg^{2+} ions, addition of the metabolite led to the appearance of five uridine imino crosspeaks (blue) at ~11.2, 12.6, 13,1, 13.4 and 14.2 ppm and caused the disappearance of the weak uridine imino peak in the absence of both Mg^{2+} and the metabolite, suggesting a tremendous conformational change and the evolution to a well-folded structure (Figure 6c). Titration of the RNA with Mg^{2+} in the presence of the metabolite shows little change in the guanine imino proton region. However, the $^{1}H-^{15}N$ HSQC spectrum in the uridine imino region, showed a noticeably change in the presence of both Mg^{2+} and the metabolite with the appearance of one more uridine imino signals at ~12.8 ppm (Figure 6c), indicating that Mg^{2+} triggers the formation of a new hydrogen bond in the presence of the metabolite. 2D NOESY spectrum was recorded for the unlabeled RNA in ligand-bound form to perform sequential walk (Supplementary Figure S5) and complete the assignment of imino protons (Figure 6d). Direct hydrogen bonding experiments further confirmed that metabolite binding triggers formation of new hydrogen bonds (Supplementary Figure S6). The imino proton sensitive to the presence of Mg^{2+} ion is U12 from L1 loop, demonstrating that Mg^{2+} is able to cooperatively facilitate loop/loop interactions. We suggest that Mg^{2+} ion binding to U12 likely nucleates the compaction of the elongated U state to the compact M state.

DISCUSSION

SAXS has proven to be a powerful approach for investigating the global size and shape of RNA and, in particular, for monitoring the conformational changes in the structure of a riboswitch upon binding metabolite (67–70). SAXS analysis in combination with NMR spectroscopy enables the resolution of global structures of

large RNA and RNA complexes into the underlying secondary and tertiary structural constituents (37,59). Therefore, we used SAXS to monitor the conformational changes of the SAM-II riboswitch in the absence or presence of Mg^{2+} and the metabolite, and NMR to pinpoint elements of structure involved in the global conformational changes. Our SAXS and NMR studies on SAM-II riboswitch combined with biochemical results suggest a model of RNA folding and functional mechanism that is characterized by an ensemble of non-native but competent conformations for ligand recognition (Figure 7). After transcription, the RNA likely adopts an elongated conformation (U state, with a R_g of ~32 Å) at low salt condition (50 mM Na^+). At physiological condition with Mg^{2+} ion in the low millimolar concentration range, the unfolded RNA collapses to the M state.

The RNA in M state samples a restricted ensemble of conformations with pairwise NSD values from 0.58 to 0.71, including conformations resembling the B and N states. This inference is supported by the similarity of the global shape of the bead model to the two states (Figure 5a). The 3′ terminus of the RNA folds back to form a pseudoknot-like conformation via tertiary contacts or Mg^{2+}-mediated electrostatic interactions with the L1 loop region of the RNA. Base pair(s) is (are) formed in the process. The exchange between open and transient close conformations of the M state RNA, however, is so fast that the temporarily formed, dynamical base pair(s) of the RNA is broadened as suggested by the induced, weak but still visible imino signal at 13.6 ppm in Figure 6a. SAM-II riboswitch samples different conformations on the nanosecond timescale based on a recent molecular dynamic simulation study (26). The RNA with this conformation in M state is also somewhat similar to what is described as the sensing phase by Stoddard *et al.* (27), and likely monitors the cellular environment for the presence of SAM metabolite to adopt a conformation that is favorable for ligand binding.

A previous smFRET study of SAM-II riboswitch suggested a stepwise global rearrangement on Mg^{2+} ion and substrate binding (36). Our SAXS studies now provide direct insight into the nature of the global conformational changes that accompany these binding events. In the presence of low millimolar concentration of Mg^{2+} ion, the closed conformation becomes increasingly

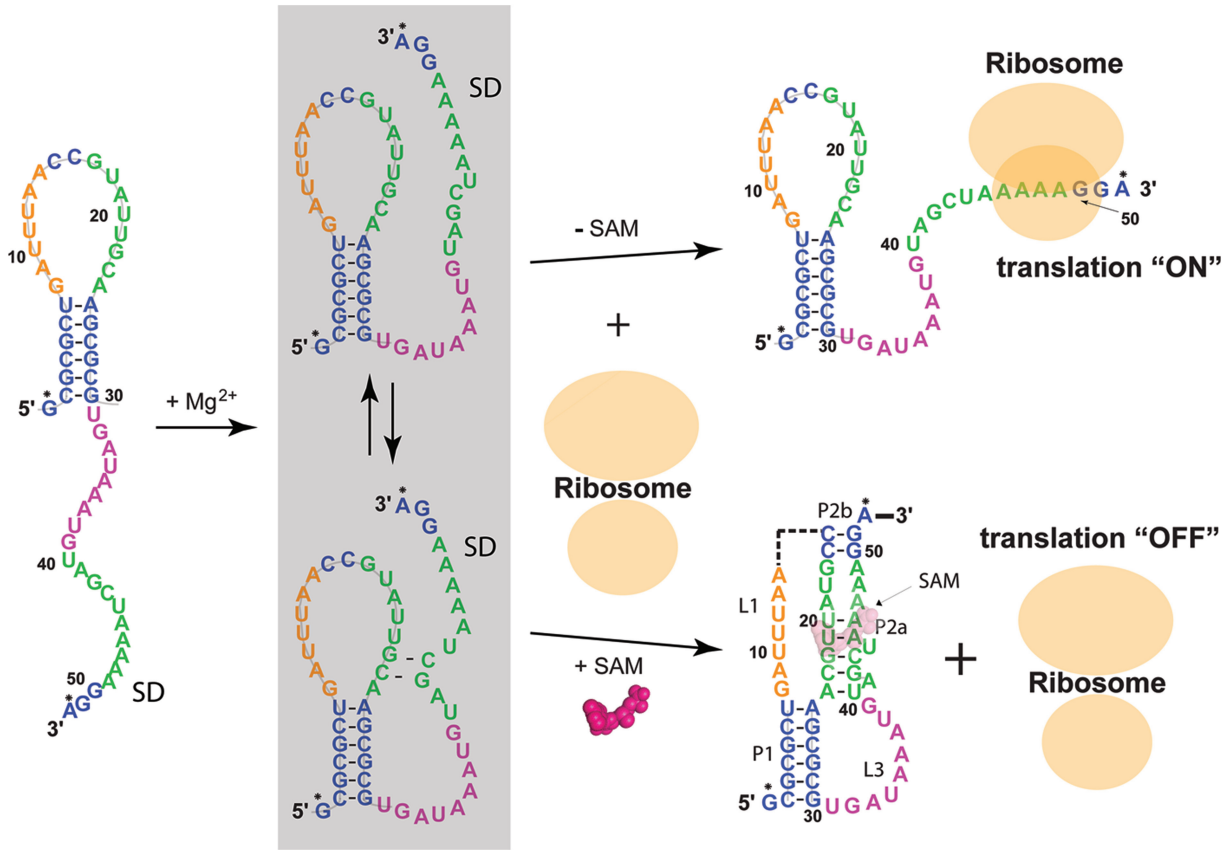

Figure 7. Schematic representation of the regulatory model of the SAM-II riboswitch. Under physiological condition, the transcribed RNA samples an ensemble of conformations with its 3′ tail folded back to get close to the L1 loop *via* unidentified Mg^{2+}-mediated electrostatic interactions. Base pairs might be formed between the 3′-tail and L1 loop region during the process to form a competent conformation favorable for ligand binding with the SD sequence being accessible for ribosome. The open/close process is so dynamic that the formed base pairs are broadened beyond observation. In the absence of the ligand, ribosome recognizes and binds the ribosomal binding site. The translation is 'ON'. In the presence of the metabolite, base paring of regions (highlighted in green and blue) forms the P2a and P2b secondary structure. Consequently, the SD sequence is sequestered and the translation is 'OFF'.

populated (36). The M state *ab initio* model is consistent with the state III of the most recent model derived from fluorescence studies of SAM-II riboswitch (36) and provides direct evidence to support the recently proposed mechanism of biomolecular recognition designated as 'conformation selection' or 'conformation capture' (34,36,71–74). On one hand, in the absence of the metabolite, the ribosome can gain access to recognize and bind the SD sequence and the translation is turned 'ON'. On the other hand, in the presence of the metabolite, ligand binding causes RNA compaction to form a new set of base pairs that appear absent or sparsely populated in the M state. As a result, the ribosomal binding site is occluded and inaccessible to ribosome. The translation is turned 'OFF' (Figure 7). The step of ligand binding to switch the RNA from M state to N state is believed to be rate-limiting since bringing several parts together to form a complex binding pocket requires overcoming an entropic barrier. Currently, there is no data available for determining whether this process is driven thermodynamically or kinetically.

Mg^{2+} ion induced compaction of the unbound SAM-II riboswitch from gel filtration studies on FPLC indicated that the Mg^{2+} concentration midpoint for the RNA compaction is ~6 mM, which is ~2–3× higher than that required for forming pseudoknot-like conformation (36). In fact, SAXS data was also collected at 2 mM Mg^{2+} ion concentration, and the *ab initio* low resolution model is quite similar to the M state model, suggesting that the unbound SAM-II riboswitch in the presence of 2 mM Mg^{2+} ion also adopts a similar ensemble of conformations with pseudoknot-like conformers (Supplementary Figure S2). In the presence of the metabolite alone without Mg^{2+} (B state), the imino $^{1}H-^{15}N$ HSQC spectrum of the RNA shows the presence of new signals corresponding to uridine imino protons with good spectral dispersion, indicating a well-folded conformation. But, compared with the spectrum in the presence of both Mg^{2+} and the metabolite, there are fewer uridine imino peaks indicative of less base pairing interactions and suggestive that the RNA in B state adopts a relatively less stable conformation. Even though the RNA has higher degree of protection by the newly formed base pairs around the metabolite induced binding pocket than that of the unfolded state, it retains some flexibility due to the absence of key A–U base pairs or Mg^{2+}-stabilized electrostatic interactions. Surprisingly, the U12 region in L1 loop is heavily perturbed by Mg^{2+} ion as exhibited by the induced formation of new base pairing interaction in the presence of Mg^{2+}, indicating that Mg^{2+} can promote loop/stem tertiary interactions. This experiment demonstrates unambiguously that, in addition to the metabolite, the Mg^{2+} ion is also required for the RNA to adopt its well-organized native folded structure. In the crystal structure of SAM-II riboswitch, a magnesium ion is positioned in a pocket formed between the 5′ termini from two RNA molecules. This magnesium ion binding site is far away from the metabolite binding pocket, suggestive of a delocalized ion binding site. However, based on our NMR data, it is likely that there is a specific magnesium binding site near this triple helix region where the ligand binding pocket is formed. Circular dichroism (CD) data also confirmed that Mg^{2+} is able to improve ligand binding affinity (B. Chen and T.K. Dayie, unpublished data). Thus, our studies indicate that Mg^{2+} and metabolite binding may act together to populate a conformation that is competent ultimately for turning off translation.

In the past studies of purine riboswitch aptamer domain using smFRET, 2-aminopurine fluorescence, force extension experiments, SHAPE, nuclease mapping and NMR (28,75–79) arrived at different conclusions about the nature of the free and bound states. These differing conclusions likely reflect the use of techniques that probed either local or global conformational changes, but not both in the same study. Our studies here using both SAXS and NMR provide a unified view of the nature of the free and bound states of SAM-II that are consistent with previous X-ray crystallography, chemical probing and smFRET data (23,36).

In summary, our data demonstrate that the SAM-II riboswitch adopts multiple conformations along its folding pathway and that under physiological conditions, the RNA is unstructured in the absence of the ligand. Addition of the metabolite induces the formation of a complicated binding pocket with the putative SD sequence of the RNA sequestered as well as extensive tertiary interactions between the RNA and the metabolite. Mg^{2+} ion is an essential cofactor for proper folding of the RNA and can facilitate the formation of a well-organized tertiary structure. Occlusion of the SD sequence is postulated to inhibit ribosomal binding and to prevent translation initiation. Our work complements and extends recent studies in two important aspects. First, SAXS provides unambiguous evidence for at least four conformational states of varying compactions, with 'Mg^{2+} only' induced compaction comparable with both 'metabolite only' and 'metabolite and Mg^{2+}' induced compactions; although the underlying secondary and tertiary structural arrangements are not completely identical. This suggests that the Mg^{2+} compacted state samples the 'metabolite and Mg^{2+} induced states in agreement with prevalent ideas about conformational selection as a basis for RNA molecular recognition (73,80). NMR analysis provides greater insights into the nature of secondary and tertiary structural rearrangement of the RNA in the presence of Mg^{2+} and metabolite, suggesting that the metabolite binding drives the folded conformer to populate the final state competent for shutting down protein synthesis.

SUPPLEMENTARY DATA

Supplementary Data are available at NAR Online: Supplementary Figures 1–6.

ACKNOWLEDGEMENTS

National Cancer Institute and Beamline 12-ID at Argonne National Laboratory. The authors also thank Dr Robert T. Batey for kindly providing the plasmid. DE-AC02-06CH11357). The authors thank X-ray

scattering beam time resource through PUP-21086/22978 between Office of Science by Argonne National Laboratory, was supported by the US DOE (under Contract No. Use of the Advanced Photon Source, an Office of Science User Facility operated for the US Department of Energy (DOE).

FUNDING

University of Maryland Nano-Biotechnology Award (partial); National Institutes of Health grant (GM077326 to T.K.D., partial). Funding for open access charge: NIH.

Conflict of interest statement. None declared.

REFERENCES

1. Mandal,M. and Breaker,R.R. (2004) Gene regulation by riboswitches. *Nat. Rev. Mol. Cell Biol.*, **5**, 451–463.
2. Hartl,D.L. and Jones,E.W. (2004) *Genetics: Analysis of Genes and Genomes*, 6 ed. Jones & Bartlett, Sudbury, MA.
3. Monod,J., Changeux,J.P. and Jacob,F. (1963) Allosteric proteins and cellular control systems. *J. Mol. Biol.*, **6**, 306–329.
4. Winkler,W., Nahvi,A. and Breaker,R.R. (2002) Thiamine derivatives bind messenger RNAs directly to regulate bacterial gene expression. *Nature*, **419**, 952–956.
5. Mandal,M., Lee,M., Barrick,J.E., Weinberg,Z., Emilsson,G.M., Ruzzo,W.L. and Breaker,R.R. (2004) A glycine-dependent riboswitch that uses cooperative binding to control gene expression. *Science*, **306**, 275–279.
6. Winkler,W.C. (2005) Riboswitches and the role of noncoding RNAs in bacterial metabolic control. *Curr. Opin. Chem. Biol.*, **9**, 594–602.
7. Roth,A. and Breaker,R.R. (2009) The structural and functional diversity of metabolite-binding riboswitches. *Annu. Rev. Biochem.*, **78**, 305–334.
8. Montange,R.K. and Batey,R.T. (2008) Riboswitches: emerging themes in RNA structure and function. *Annu. Rev. Biophys.*, **37**, 117–133.
9. Tucker,B.J. and Breaker,R.R. (2005) Riboswitches as versatile gene control elements. *Curr. Opin. Struct. Biol.*, **15**, 342–348.
10. Coppins,R.L., Hall,K.B. and Groisman,E.A. (2007) The intricate world of riboswitches. *Curr. Opin. Microbiol.*, **10**, 176–181.
11. Mandal,M. and Breaker,R.R. (2004) Adenine riboswitches and gene activation by disruption of a transcription terminator. *Nat. Struct. Mol. Biol.*, **11**, 29–35.
12. Serganov,A. (2009) The long and the short of riboswitches. *Curr. Opin. Struct. Biol.*, **19**, 251–259.
13. Breaker,R.R. (2008) Complex riboswitches. *Science*, **319**, 1795–1797.
14. Batey,R.T., Gilbert,S.D. and Montange,R.K. (2004) Structure of a natural guanine-responsive riboswitch complexed with the metabolite hypoxanthine. *Nature*, **432**, 411–415.
15. Dann,C.E. III, Wakeman,C.A., Sieling,C.L., Baker,S.C., Irnov,I. and Winkler,W.C. (2007) Structure and mechanism of a metal-sensing regulatory RNA. *Cell*, **130**, 878–892.
16. Thore,S., Leibundgut,M. and Ban,N. (2006) Structure of the eukaryotic thiamine pyrophosphate riboswitch with its regulatory ligand. *Science*, **312**, 1208–1211.
17. Montange,R.K. and Batey,R.T. (2006) Structure of the S-adenosylmethionine riboswitch regulatory mRNA element. *Nature*, **441**, 1172–1175.
18. Cochrane,J.C., Lipchock,S.V. and Strobel,S.A. (2007) Structural investigation of the GlmS ribozyme bound to Its catalytic cofactor. *Chem. Biol.*, **14**, 97–105.
19. Serganov,A., Polonskaia,A., Phan,A.T., Breaker,R.R. and Patel,D.J. (2006) Structural basis for gene regulation by a thiamine pyrophosphate-sensing riboswitch. *Nature*, **441**, 1167–1171.
20. Serganov,A., Huang,L. and Patel,D.J. (2009) Coenzyme recognition and gene regulation by a flavin mononucleotide riboswitch. *Nature*, **458**, 233–237.
21. Kang,M., Peterson,R. and Feigon,J. (2009) Structural Insights into riboswitch control of the biosynthesis of queuosine, a modified nucleotide found in the anticodon of tRNA. *Mol. Cell*, **33**, 784–790.
22. Serganov,A., Huang,L. and Patel,D.J. (2008) Structural insights into amino acid binding and gene control by a lysine riboswitch. *Nature*, **455**, 1263–1267.
23. Gilbert,S.D., Rambo,R.P., Van Tyne,D. and Batey,R.T. (2008) Structure of the SAM-II riboswitch bound to S-adenosylmethionine. *Nat. Struct. Mol. Biol.*, **15**, 177–182.
24. Lipfert,J., Das,R., Chu,V.B., Kudaravalli,M., Boyd,N., Herschlag,D. and Doniach,S. (2007) Structural transitions and thermodynamics of a glycine-dependent riboswitch from Vibrio cholerae. *J. Mol. Biol.*, **365**, 1393–1406.
25. Ali,M., Lipfert,J., Seifert,S., Herschlag,D. and Doniach,S. (2010) The ligand-free state of the TPP riboswitch: a partially folded RNA structure. *J. Mol. Biol.*, **396**, 153–165.
26. Kelley,J.M. and Hamelberg,D. (2010) Atomistic basis for the on-off signaling mechanism in SAM-II riboswitch. *Nucleic Acids Res.*, **38**, 1392–1400.
27. Stoddard,C.D., Montange,R.K., Hennelly,S.P., Rambo,R.P., Sanbonmatsu,K.Y. and Batey,R.T. (2010) Free state conformational sampling of the SAM-I riboswitch aptamer domain. *Structure*, **18**, 787–797.
28. Ottink,O.M., Rampersad,S.M., Tessari,M., Zaman,G.J., Heus,H.A. and Wijmenga,S.S. (2007) Ligand-induced folding of the guanine-sensing riboswitch is controlled by a combined predetermined induced fit mechanism. *RNA*, **13**, 2202–2212.
29. Sudarsan,N., Wickiser,J.K., Nakamura,S., Ebert,M.S. and Breaker,R.R. (2003) An mRNA structure in bacteria that controls gene expression by binding lysine. *Genes Dev.*, **17**, 2688–2697.
30. Garst,A.D., Heroux,A., Rambo,R.P. and Batey,R.T. (2008) Crystal structure of the lysine riboswitch regulatory mRNA element. *J. Biol. Chem.*, **283**, 22347–22351.
31. Rieder,U., Kreutz,C. and Micura,R. (2010) Folding of a transcriptionally acting PreQ1 riboswitch. *Proc. Natl Acad. Sci. USA*, **107**, 10804–10809.
32. Fuchs,R.T., Grundy,F.J. and Henkin,T.M. (2007) S-adenosylmethionine directly inhibits binding of 30S ribosomal subunits to the SMK box translational riboswitch RNA. *Proc. Natl Acad. Sci. USA*, **104**, 4876–4880.
33. Smith,A.M., Fuchs,R.T., Grundy,F.J. and Henkin,T.M. (2010) The SAM-responsive SMK box is a reversible riboswitch. *Mol. Microbiol.*, **78**, 1393–1402.
34. Wilson,R.C., Smith,A.M., Fuchs,R.T., Kleckner,I.R., Henkin,T.M. and Foster,M.P. (2011) Tuning riboswitch regulation through conformational selection. *J Mol. Biol.*, **405**, 926–938.
35. Corbino,K.A., Barrick,J.E., Lim,J., Welz,R., Tucker,B.J., Puskarz,I., Mandal,M., Rudnick,N.D. and Breaker,R.R. (2005) Evidence for a second class of S-adenosylmethionine riboswitches and other regulatory RNA motifs in alpha-proteobacteria. *Genome Biol*, **6**, R70.
36. Haller,A., Rieder,U., Aigner,M., Blanchard,S.C. and Micura,R. (2011) Conformational capture of the SAM-II riboswitch. *Nat Chem Biol*, **7**, 393–400.
37. Wang,Y., Zuo,X., Wang,J., Yu,P. and Butcher,S.E. (2010) Rapid global structure determination of large RNA and RNA complexes using NMR and small-angle X-ray scattering. *Methods*, **52**, 180–191.
38. Wang,J., Zuo,X., Yu,P., Byeon,I.J., Jung,J., Wang,X., Dyba,M., Seifert,S., Schwieters,C.D., Qin,J. *et al.* (2009) Determination of multicomponent protein structures in solution using global orientation and shape restraints. *J. Am. Chem. Soc.*, **131**, 10507–10515.
39. Svergun,D.I. (1992) Determination of the regularization parameter in indirect-transform methods using perceptual criteria. *J Appl Crystallogr.*, **25**, 495–503.
40. Svergun,D.I. (1999) Restoring low resolution structure of biological macromolecules from solution scattering using simulated annealing. *Biophys. J.*, **76**, 2879–2886.

41. Volkov,V.V. and Svergun,D.I. (2003) Uniqueness of ab initio shape determination in small-angle scattering. *J. Appl. Cryst.*, **36**, 860–864.
42. Svergun,D.I., Barberato,C. and Koch,M.H.J. (1995) CRYSOL—a program to evaluate X-ray solution scattering of biological macromolecules from atomic coordinates. *J. Appl. Cryst.*, **28**, 768–773.
43. Piotto,M., Saudek,K. and Sklenár,V. (1992) Gradient-tailored excitation for single-quantum NMR spectroscopy of aqueous solutions. *J. Biomol. NMR*, **2**, 661–665.
44. Sklenar,V., Peterson,R.D., Rejante,M.R. and Feigon,J. (1994) Correlation of nucleotide base and sugar protons in a ^{15}N-labeled HIV-1 RNA oligonucleotide by ^{1}H-^{15}N HSQC experiments. *J. Biomol. NMR*, **4**, 117–122.
45. Wijmenga,S.S. and van Buuren,B.N.M. (1998) The use of NMR methods for conformational studies of nucleic acids. *Prog. NMR Spectrosc.*, **32**, 287–387.
46. Dingley,A.J. and Grzesiek,S. (1998) Direct observation of hydrogen bonds in nucleic acid base pairs by internucleotide 2JNN couplings. *J. Am. Chem. Soc.*, **120**, 8293–8297.
47. Delaglio,F., Grzesiek,S., Vuister,G.W., Zhu,G., Pfeifer,J. and Bax,A. (1995) NMRPipe: a multidimensional spectral processing system based on UNIX pipes. *J. Biomol. NMR*, **6**, 277–293.
48. Johnson,B.A. and Blevins,R.A. (1994) NMRView: a computer program for the visualization and analysis of NMR data. *J. Biomol. NMR*, **4**, 603–614.
49. Dayie,T.K. (2008) Key labeling technologies to tackle sizeable problems in RNA structural biology. *Int. J. Mol. Sci.*, **9**, 1214–1240.
50. Lukavsky,P.J. and Puglisi,J.D. (2004) Large-scale preparation and purification of polyacrylamide-free RNA oligonucleotides. *RNA*, **10**, 889–893.
51. Rambo,R.P. and Tainer,J.A. (2010) Improving small-angle X-ray scattering data for structural analysis of the RNA world. *RNA*, **16**, 638–646.
52. Treiber,D.K. and Williamson,J.R. (1999) Exposing the kinetic traps in RNA folding. *Curr. Opin. Struct. Biol.*, **9**, 339–345.
53. Treiber,D.K. and Williamson,J.R. (2001) Beyond kinetic traps in RNA folding. *Curr. Opin. Struct. Biol.*, **11**, 309–314.
54. Hura,G.L., Menon,A.L., Hammel,M., Rambo,R.P., Poole,F.L. II, Tsutakawa,S.E., Jenney,F.E. Jr, Classen,S., Frankel,K.A., Hopkins,R.C. *et al.* (2009) Robust, high-throughput solution structural analyses by small angle X-ray scattering (SAXS). *Nat. Meth.*, **6**, 606–612.
55. Kim,I., McKenna,S.A., Viani Puglisi,E. and Puglisi,J.D. (2007) Rapid purification of RNAs using fast performance liquid chromatography (FPLC). *RNA*, **13**, 289–294.
56. Cann,J.R. (1996) Theory and practice of gel electrophoresis of interacting macromolecules. *Anal. Biochem.*, **237**, 1–16.
57. Woodson,S.A. and Koculi,E. (2009) Analysis of RNA folding by native polyacrylamide gel electrophoresis. In: Daniel,H. (ed.), *Methods in Enzymology. Biophysical, Chemical, and Functional Probes of RNA Structure, Interactions and Folding: Part B.* Academic Press, San Diego CA, pp. 189–208.
58. Doniach,S. (2001) Changes in biomolecular conformation seen by small angle X-ray scattering. *Chem. Rev.*, **101**, 1763–1778.
59. Zuo,X., Wang,J., Foster,T.R., Schwieters,C.D., Tiede,D.M., Butcher,S.E. and Wang,Y. (2008) Global molecular structure and interfaces: refining an RNA:RNA complex structure using solution X-ray scattering data. *J. Am. Chem. Soc.*, **130**, 3292–3293.
60. Chu,V.B., Bai,Y., Lipfert,J., Herschlag,D. and Doniach,S. (2008) A repulsive field: advances in the electrostatics of the ion atmosphere. *Curr. Opin. Chem. Biol.*, **12**, 619–625.
61. Wong,G.C. and Pollack,L. (2010) Electrostatics of strongly charged biological polymers: ion-mediated interactions and self-organization in nucleic acids and proteins. *Annu. Rev. Phys. Chem.*, **61**, 171–189.
62. Woodson,S.A. (2010) Compact intermediates in RNA folding. *Annu. Rev. Biophys.*, **39**, 61–77.
63. Draper,D.E. (2008) RNA folding: thermodynamic and molecular descriptions of the roles of ions. *Biophys. J.*, **95**, 5489–5495.
64. Kozin,M.B. and Svergun,D.I. (2001) Automated matching of high- and low-resolution structural models. *J Appl Cryst.*, **34**, 33–41.
65. Lipfert,J., Sim,A.Y.L., Herschlag,D. and Doniach,S. (2010) Dissecting electrostatic screening, specific ion binding, and ligand binding in an energetic model for glycine riboswitch folding. *RNA*, **16**, 708–719.
66. Seetharaman,M.A.H.A., Eldho,N.V., Padgett,R.A. and Dayie,K.T. (2006) Structure of a self-splicing group II intron catalytic effector domain 5: parallels with spliceosomal U6 RNA. *RNA*, **12**, 235–247.
67. Russell,R., Ian,S., Millett,I.S., Doniach,S. and Herschlag,D. (2000) Small angle X-ray scattering reveals a compact intermediate in RNA folding. *Nat. Struct. Mol. Biol.*, **7**, 367–370.
68. Baird,N.J. and Ferre-D'Amare,A.R. (2010) Idiosyncratically tuned switching behavior of riboswitch aptamer domains revealed by comparative small-angle X-ray scattering analysis. *RNA*, **16**, 598–609.
69. Doniach,S. and Lipfert,J. (2009) Use of small angle X-ray scattering (SAXS) to characterize conformational states of functional RNAs. *Methods Enzymol.*, **469**, 237–251.
70. Russell,R., Millett,I.S., Tate,M.W., Kwok,L.W., Nakatani,B., Gruner,S.M., Mochrie,S.G.J., Pande,V., Doniach,S., Herschlag,D. *et al.* (2002) Rapid compaction during RNA folding. *Proc. Natl Acad. Sci. USA*, **99**, 4266–4271.
71. Leulliot,N. and Varani,G. (2001) Current topics in RNA-protein recognition: control of specificity and biological function through induced fit and conformational capture. *Biochemistry*, **40**, 7947–7956.
72. Boehr,D.D., Nussinov,R. and Wright,P.E. (2009) The role of dynamic conformational ensembles in biomolecular recognition. *Nat Chem Biol*, **5**, 789–796.
73. Hammes,G.G., Chang,Y.C. and Oas,T.G. (2009) Conformational selection or induced fit: a flux description of reaction mechanism. *Proc. Natl Acad. Sci. USA*, **106**, 13737–13741.
74. Hermann,T. and Patel,D.J. (2000) Adaptive recognition by nucleic acid aptamers. *Science*, **287**, 820–825.
75. Noeske,J., Schwalbe,H. and Wohnert,J. (2007) Metal-ion binding and metal-ion induced folding of the adenine-sensing riboswitch aptamer domain. *Nucleic Acids Res.*, **35**, 5262–5273.
76. Noeske,J., Buck,J., Furtig,B., Nasiri,H.R., Schwalbe,H. and Wohnert,J. (2007) Interplay of 'induced fit' and preorganization in the ligand induced folding of the aptamer domain of the guanine binding riboswitch. *Nucleic Acids Res.*, **35**, 572–583.
77. Stoddard,C.D., Gilbert,S.D. and Batey,R.T. (2008) Ligand-dependent folding of the three-way junction in the purine riboswitch. *RNA*, **14**, 675–684.
78. Rieder,R., Lang,K., Graber,D. and Micura,R. (2007) Ligand-induced folding of the adenosine deaminase A-riboswitch and implications on riboswitch translational control. *Chembiochem*, **8**, 896–902.
79. Lemay,J.F., Penedo,J.C., Tremblay,R., Lilley,D.M. and Lafontaine,D.A. (2006) Folding of the adenine riboswitch. *Chem. Biol.*, **13**, 857–868.
80. Zhang,Q. and Al-Hashimi,H.M. (2009) Domain-elongation NMR spectroscopy yields new insights into RNA dynamics and adaptive recognition. *RNA*, **15**, 1941–1948.